Linear instability and weakly nonlinear effects in eastward dipoles

J. Davies [a],[*], I. Shevchenko [a],[b], P. Berloff [a],[c], G.G. Sutyrin [d]

[a] *Department of Mathematics, Imperial College London, London SW7 2AZ, UK*
[b] *National Oceanography Centre, European Way, Southampton, SO14 3ZH, UK*
[c] *Institute of Numerical Mathematics, Russian Academy of Sciences, Moscow, Russia*
[d] *Graduate School of Oceanography, University of Rhode Island, Narragansett 02882, USA*

ARTICLE INFO

ABSTRACT

The linear instability and weakly nonlinear dynamics of eastward-propagating, steady-state Larichev–Reznik vortex dipoles are explored in terms of two-dimensional normal-mode analysis. To extract the fastest growing normal modes, we apply both breeding methodology based on solving the initial-value problem, as well as a direct-solution approach through the full-spectrum eigenproblem involving large matrices. We find that the amplification rate of dipole instability decreases with respect to increase in dipole intensity. In our study, both approaches yield consistent results and are systematically compared to provide guidance for further studies of vortex structures.

We consider nonlinear self-interaction of the fastest growing mode, along with the induced eddy fluxes, their divergence and mechanical energy balance. Through this analysis, we find that the unstable mode leads to weakening of the dipole by extracting its energy and exchanging potential vorticity content in the down-gradient sense, thus, providing a nonlinear physical mechanism for the dipole destruction. In particular, we highlight the fundamental importance of the west-east asymmetry of the normal mode for destruction to be realized. In summary, we consider this work to be a foundational demonstration of useful methodology for future studies of dynamics and stability of isolated vortices without simplifying spatial symmetries, such as ubiquitous vortices in geophysical fluids.

1. Introduction

Dynamics of isolated coherent vortices has been a subject extensively studied with applications to oceanic [1–3] and atmospheric [4–6] settings. These vortices transport and redistribute important fluid properties, such as heat, momentum and material tracers, and therefore largely shape up general circulations. Taxonomy, generation, dynamics, life cycles and impacts of the vortices remain only partially understood despite many decades of research.

A common vortex representation is the class of vortex dipoles, those being eddy pairs of opposite vorticity sign. An example of which is the Lamb–Chaplygin dipole (LCD) [7,8], which is a steady-state solution to the two-dimensional (2D) Euler equations. In the absence of viscosity, the LCD exhibits slow evolution towards a smoother vorticity profile with elliptical deviation in the initially circular separatrix [9]. The LCD is not an exact solution to the 2D Euler equations in the addition of viscosity, and it is also unstable when exposed to small perturbations [10]. Different dipoles are found in other systems, including the classical quasigeostrophic (QG) equivalent-barotropic model on the β-plane (describing fluids on rotating spheres). In particular, a stationary

solution derived by Stern [11] was found to be unstable [12], while another solution with steady zonal (along latitudes) propagation was found analytically, as the so-called Larichev–Reznik dipole or LRD [13].

The LRD solutions can propagate in either eastward or westward directions, provided the Rossby deformation radius is finite. The propagation speed is unbounded for eastward dipoles, but for the westward ones it must exceed the maximum Rossby wave phase speed [14]. Westward propagating LRDs were suggested as a model for atmospheric blocking [15,16], however, because of their intrinsic instability [17] and rapid disintegration, this idea was later abandoned. Various studies suggested that eastward LRDs may be stable, when exposed to weak frictional effects [18], short-wave disturbances [19] and topographic perturbations [20], but rigorous proof of either stability or instability of eastward dipoles remains to be found [17,21,22].

Recently, high-resolution numerical modelling of the eastward LRD evolution demonstrated that over some time the dipole experiences the phenomenon of spontaneous symmetry breaking, which triggers exponentially growing oscillation and leads to the eventual break-up of the structure into two monopolar vortices. As these drift apart, they

---

* Corresponding author.
E-mail address: jack.davies18@imperial.ac.uk (J. Davies).

start propagating (in the opposite direction) to the west and eventually disintegrate into the background flow [23]. The main focus of our study is in understanding the involved dynamical mechanism that results in the inevitable dipole destruction. Note that the instability scenario is further supported by [24], which considered evolution of LRDs initially tilted away from their zonal alignment. A conclusion of these studies was that the development of a critical instability mode (a so-called A-mode or D-mode) introduced asymmetry that played into the inevitable destruction of the eddy pair.

Another useful part of the background is to remind readers that we will solve a large eigenproblem by a direct brute-force approach, yielding the D-mode. For vortices with azimuthal symmetry, the eigenproblem can be formulated separately for each angular mode and solved with small computational cost [25]; however, we do not consider this setup in this study, and such a framework is not representative of more general vortices. Large eigenproblems for QG dynamics and stability analysis have been considered in the past [26].

The main motivations of our study are to extract the growing instability in terms of the D-mode and to understand the mechanisms by which this mode destroys the dipole. We introduce the model assumptions and set up the problem in §2. Continuing from this, in §3, we carry out linear instability analyses for various parameters and LRD intensities, thus, extracting critical normal modes. In §4 we explore the nonlinear mechanism that involves nonlinear self-interaction of the critical mode and explains the inevitable dipole destruction. We show that the critical unstable mode extracts energy from the LRD and irreversibly stirs its potential vorticity (PV) content, thus, reducing dipole intensity. Next we demonstrate that the above mechanisms are a consequence of the east–west asymmetry of the critical mode structure. Finally, we conclude the study in §5 and discuss further routes of progression.

2. Model assumptions

2.1. QG dynamics

In the studies [23,24], which are prequels to this work, an equivalent-barotropic quasigeostrophic (QG) model on the planetary β-plane was utilized to study the dynamics of eastward propagating LRDs. The governing equation nondimensionalized with the length and velocity scales, L and U, respectively, is [27,28]:

$$\mathscr{D}_t \Pi = \frac{1}{Re} \nabla^4 \psi \,, \qquad (1)$$
$$\Pi = q + \beta Y \,,$$

where (X, Y) denote conventional horizontal coordinates, t denotes time, β is the meridional gradient of the Coriolis parameter, Re is the Reynolds number; the potential vorticity anomaly (PVA) is defined as

$$q(X, Y, t) = \nabla^2 \psi - \gamma^2 \psi \,, \qquad (2)$$

where $\psi(X, Y, t)$ is the velocity streamfunction, γ describes the ratio of the arbitrary length scale to the Rossby deformation radius, and $\Pi(X, Y, t)$ is the full PV field. In our notation, we use the following differential operators:

$$\mathscr{D}_t := \partial_t - \partial_Y \psi \partial_X + \partial_X \psi \partial_Y \,, \qquad (3)$$
$$\nabla^2 := \partial_{XX} + \partial_{YY} \,,$$

where ∂_z is the derivative with respect to the variable z. We impose an isolated vortex centred at (x_c, y_c) and introduce the change of variables

$$x = X - x_c(t) \,, \qquad (4)$$
$$y = Y - y_c(t) \,,$$

which centres our reference frame with the vortex. This yields the governance

$$\partial_t q + \mathscr{J}(\psi + \partial_t x_c y - \partial_t y_c x, q + \beta y) = \frac{1}{Re} \Delta^2 \psi \,, \qquad (5)$$

where we define the Jacobian operator of functions $a(x, y)$ and $b(x, y)$ as

$$\mathscr{J}(a, b) = \partial_x a \partial_y b - \partial_y a \partial_x b \,, \qquad (6)$$

and

$$\Delta := \partial_{xx} + \partial_{yy} \,. \qquad (7)$$

2.2. Symmetry decomposition

Due to the base flow symmetry, the streamfunction field in the domain can be uniquely divided into two components, following [23]:

$$\psi_A = \frac{\psi(x, y, t) + \psi(x, -y, t)}{2} \,, \qquad (8)$$
$$\psi_S = \frac{\psi(x, y, t) - \psi(x, -y, t)}{2} \,,$$

where ψ_A is A-component, which has even symmetry relative to the zonal axis, and ψ_S is S-component, which has odd symmetry relative to the zonal axis. The interpretation of these components is the following: the S-component perturbation leads to symmetric deformation of the vortices around the zonal axis, whereas, the A-component perturbation leads to the antisymmetric deformation of the vortices.

The quadratic invariants of energy and enstrophy for each component are obtained by means of integration:

$$E_{A,S} = \frac{1}{2} \int_\Sigma \left[(\nabla \psi_{A,S})^2 + \gamma^2 \psi_{A,S}^2 \right] \, \mathrm{d}\Sigma \,, \qquad (9)$$
$$Z_{A,S} = \frac{1}{2} \int_\Sigma q_{A,S}^2 \, \mathrm{d}\Sigma \,,$$

where Σ denotes a domain of integration and $\mathrm{d}\Sigma = \mathrm{d}x \, \mathrm{d}y$, the A- and S-component of the PVA field are given by

$$q_{A,S} = \Delta \psi_{A,S} - \gamma^2 \psi_{A,S} \,, \qquad (10)$$

and the summations $E_A + E_S$ and $Z_A + Z_S$ are conserved for the inviscid case (i.e., $Re \to \infty$).

Hereafter, we assume the inviscid limit since we are interested in solutions to the inviscid fluid governance (i.e., see in Appendix A1 with RHS equal to zero). This is justified by the sensitivity analysis carried out in [23], however, the linear instability methodology below is applicable even if we consider finite Reynolds number.

2.3. LRD steady states

To explore the dynamics of steady-state dipole solutions, we set $\partial_t q = 0$, so that the QG system becomes

$$\mathscr{J}(\psi + c_x y - c_y x, q + \beta y) = 0 \,, \qquad (11)$$

where $c_{x,y}$ denote constant drifts of the dipole in the zonal and meridional directions, respectively. The class of LRDs are steady-state solutions to (5) in the inviscid limit with $c_y = 0$, over an infinite domain. More specifically, these are derived from the relative-vorticity relation,

$$\Delta \psi = \begin{cases} -k^2 \psi - c(k^2 + p^2) r \sin \vartheta, & r \le 1 \,, \\ p^2 \psi, & r > 1 \,, \end{cases} \qquad (12)$$

where $c = c_x$; (r, ϑ) are standard polar coordinates; $r = 1$ is circular separatrix (here, L is chosen to be the horizontal vortex scale); $p^2 = \beta/c + \gamma > 0$. Here, k is some positive constant satisfying the nonlinear equation:

$$k J_1(k) K_2(p) + p K_1(p) J_2(k) = 0 \,, \qquad (13)$$

where J_μ and K_μ are the order-μ Bessel and modified Bessel functions of the first kind, respectively. This equation has an infinite number of solutions for k, but we considered only dipoles with the lowest k, being

motivated by [29], where the higher-order modes (in a surface-QG model) were found unstable.

We assume that the dipole is spatially localized, i.e., $\psi \rightarrow 0$ decays exponentially as $r \rightarrow \infty$, and the solution is continuous and continuously differentiable across the separatrix $r = 1$. With this in mind, the streamfunction field can be extracted as a profile with odd symmetry about the dipole axis:

$$\psi(r, \vartheta) = c\, f(r) \sin \vartheta \,, \tag{14}$$

where

$$f(r) = \begin{cases} (p/k)^2 (J_1(kr)/J_1(k) - r) - r, & r \le 1 \,, \\ -K_1(pr)/K_1(p), & r > 1 \,. \end{cases} \tag{15}$$

2.4. D-mode instability

The stability of eastward LRDs has been a subject of discussion in many studies [18–20], but most recently [23] employed a *breeding* method [30] in a high-resolution numerical model (equipped with the CABARET advection scheme), which resulted in the extraction of a growing A-component (a so-called critical D-mode) that was associated with the spontaneous symmetry breaking of the LRD. The breeding methodology involves the following steps:

- simulate the LRD evolution (slightly perturbed on the first iteration);
- extract the A-component field for an intermediate stage of the unstable growth;
- use this pattern to perturb the original LRD and solve dynamically for its evolution and growth;
- iterate this process several times until an accurate critical D-mode is distilled out of the growing instability.

The main benefit of this approach is the simplicity it offers, where we are required to solve an initial-value problem rather than a global problem. Furthermore, breeding efficiently makes use of a high-resolution grid, since it only yields the fastest-growing mode rather than the full normal-mode spectrum.

We can associate the D-mode with a linear instability mode of the dipole by seeking ψ_A of the following form:

$$\psi_A = (A c_1 - B s_1) e^{\sigma t} \,, \tag{16}$$

where $A(x, y)$ and $B(x, y)$ are the real and imaginary parts of the mode, respectively; $\omega = 2\pi/\tau$ is the oscillation frequency (with period of oscillation τ), σ is the linear growth rate, and

$$\begin{aligned} c_n(t) &= \cos(n\omega t) \,, \\ s_n(t) &= \sin(n\omega t) \,, \end{aligned} \tag{17}$$

for $n \in \mathbb{Z}^+$. Using (16), we can derive the corresponding average over the period, say in the interval $[t_1, t_1+\tau]$ (where t_1 is some instant during the linear instability growth) for the A-perturbation field:

$$\begin{aligned} \overline{\psi_A} &= \frac{1}{\tau} \int_{t_1}^{t_1+\tau} \psi_A \, \mathrm{d}t \\ &= \Lambda \left[(A\sigma + B\omega) c_1(t_1) + (A\omega - B\sigma) s_1(t_1) \right] e^{\sigma t_1} \,, \end{aligned} \tag{18}$$

where

$$\Lambda = \frac{1}{\tau} \left(\frac{e^{\sigma\tau} - 1}{\sigma^2 + \omega^2} \right) . \tag{19}$$

Furthermore, using periodicity, we can obtain A and B:

$$\begin{aligned} A &= \left[\psi_1 c_1(t_1) - \psi_2 s_1(t_1) e^{-\sigma\tau/4} \right] e^{-\sigma t_1} \,, \\ B &= -\left[\psi_1 s_1(t_1) + \psi_2 c_1(t_1) e^{-\sigma\tau/4} \right] e^{-\sigma t_1} \,, \end{aligned} \tag{20}$$
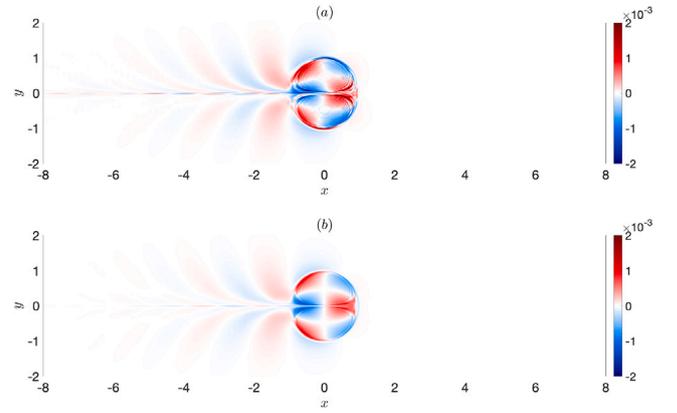
Fig. 1. Period-averaged D-mode in terms of PVA fields (multiplied by $e^{-\sigma t_1}$), corresponding to $\beta = 4c$: (*a*) is obtained by averaging bred-out model solution over the period of oscillation; (*b*) is obtained by using (21) with $\sigma \approx 0.035$ and $\tau \approx 16$. Similarity between panels (*a*) and (*b*) (spatial correlation of 0.8) motivates the direct linear-stability analysis, and also benchmarks it against the breeding method; the former is preferable but resolution-limited relative to the breeding, therefore, cross-validation of the methods is fully justified and shown to be successful.

where $\psi_1 = \psi_A(x, y, t_1)$ and $\psi_2 = \psi_A(x, y, t_1 + \tau/4)$. Therefore, we can rewrite (18) so that:

$$\overline{\psi_A} = \Lambda(\sigma\psi_1 - \omega\psi_2 e^{-\sigma\tau/4}) \,. \tag{21}$$

Due to the flow symmetry of the LRD, if the average profile of the D-mode is non-zero, when computed over a period of oscillation during an intermediate stage of growth, this corresponds to instability of the eastward dipole.

We fitted the normal mode form using q_A solutions with $\sigma \approx 0.035$ and $\tau \approx 16$ (as approximated in [23]), which enabled us to compare the analytical period-averaged field with the numerical equivalent. This comparison found reasonable similarity between these profiles (Fig. 1), with the corresponding spatial correlation coefficient $\rho = 0.8$. We checked that further refinement of the numerical grid yielded similar outcomes, hence, allowing us to conclude the adequacy of the spatial resolution of the numerical grid.

The results of Fig. 1 motivate the linear instability analysis of the LRD, which is computationally expensive and even prohibitively so for grids with a greater number of nodes. Such analysis allows for accurate extraction of σ and τ, as well as provides us with the full eigenspectra, as opposed to only obtaining the fastest growing normal mode. The latter may be important in situations when there are near-critical D-modes with similar to the critical growth rates and for non-orthogonal modes that can interact with each other [31].

In the following section, we carry out the linear instability analysis.

3. Direct linear-stability analysis

3.1. Constructing the eigenproblem

Firstly, we consider the linear perturbation equation

$$\partial_t q_A + \mathcal{J}(\psi + cy, q_A) + \mathcal{J}(\psi_A, q + \beta y) = 0 \,, \tag{22}$$

where the A-components represent growing perturbations (or in this case, correspond to the growing D-mode on the LRD). We seek complex solutions of the form

$$\begin{aligned} \psi_A(x, y, t) &= \Psi(x, y) e^{(\sigma + i\omega)t} \,, \\ q_A(x, y, t) &= Q(x, y) e^{(\sigma + i\omega)t} \,, \end{aligned} \tag{23}$$

where Ψ is the complex amplitude of the growing perturbation streamfunction, and the perturbation PV is given by

$$Q = \Delta\Psi - \gamma^2 \Psi \,. \tag{24}$$

Then, the perturbation equation becomes

$$\mathscr{J}(\psi + cy, Q) + \mathscr{J}(\Psi, q + \beta y) = i\omega Q. \tag{25}$$

We discretize (25) using second-order central finite differences, to obtain a system of difference equations on an (i, j)-grid, where i and j are the zonal and meridional nodal indices, respectively. In the prequel works [23,24], a double-periodic $(60, 15)$-domain was employed with $(8192, 2048)$ grid points. The zonally large domain size was motivated by avoiding late-time (periodic) interaction with the trailing wake, however, this is not an issue for the linear-instability analysis. Therefore, we consider a square domain with $N \in \mathbb{Z}^+$ grid points in each horizontal direction. Thus, the eigenproblem can be expressed in the matrix form

$$i\mathbf{M}\boldsymbol{\Psi} = \omega\mathbf{N}\boldsymbol{\Psi}, \tag{26}$$

where

$$\boldsymbol{\Psi} = (\Psi_{1,1}, \Psi_{1,2}, \dots, \Psi_{N,1}, \Psi_{2,1}, \dots, \Psi_{N,N})^T \in \mathbb{C}^{N^2}, \tag{27}$$

and the matrices $\mathbf{N} \in \mathbb{R}^{N^2 \times N^2}$ and $\mathbf{M} \in \mathbb{R}^{N^2 \times N^2}$ have entries detailed in Appendix A.1. Moreover, the system is equipped with doubly-periodic boundary conditions:

$$
\begin{aligned}
\Psi_{N+1,j} &= \Psi_{1,j}, \\
\Psi_{0,j} &= \Psi_{N,j}, \\
\Psi_{i,N+1} &= \Psi_{i,1}, \\
\Psi_{i,0} &= \Psi_{N,j}.
\end{aligned} \tag{28}
$$

Since the coefficient matrices in (26) quadruple in size with respect to increasing N, it is not computationally feasible to use $N = 2048$ (i.e., using the same numerical accuracy as in [23,24]). Instead, we used $N = 512$ (the extreme value we could afford given the resources) and considered a $(7.5, 7.5)$ domain (half the size of the domain employed in the model, if it were square). This resolution is achievable despite the large computational expense since we make use of D-mode antisymmetry to consider only half of the domain, where we match boundary conditions at the middle latitude. This is equivalent to imposing the additional boundary conditions:

$$
\begin{aligned}
\Psi_{i,N/2+1} &= \Psi_{i,N/2}, \\
\Psi_{i,N/2+2} &= \Psi_{i,N/2-1}, \\
&\vdots \\
\Psi_{i,N} &= \Psi_{i,1}.
\end{aligned} \tag{29}
$$

Since we halved the domain size, this is equivalent to doubling grid resolution over the smaller domain and thus provides higher accuracy.

To evaluate the merit of this approach, we carried out a solution analysis, in which we considered different domain sizes and resolutions, and deduced that $N = 512$ for a $(15, 15)$-domain is the lower-bound requirement for approximating the critical D-mode (see the supplementary material). When comparing this with solutions obtained for the same value of N but in a halved $(7.5, 7.5)$ domain, the critical D-mode retained its characteristics. Hence, we proceed by presenting the smaller domain solutions.

3.2. Linear stability results

For illustration, we consider an LRD with $\beta = 4c$ and show the real and imaginary components of the D-mode in Fig. 2. These fields are similar to those in [23], which confirms that the dipole exhibits essentially an inviscid instability, since our linear-stability formulation is inviscid (note, this is fundamentally different from the LCD viscous instability mechanism [10]).

Temporal behaviour of the D-mode is described by the pair (σ, τ), which embodies the rate of growth and the period of oscillation of the D-mode, respectively. In [23], this information was approximated using a finite number of snapshots. More specifically, during $t_1 \leq t \leq$
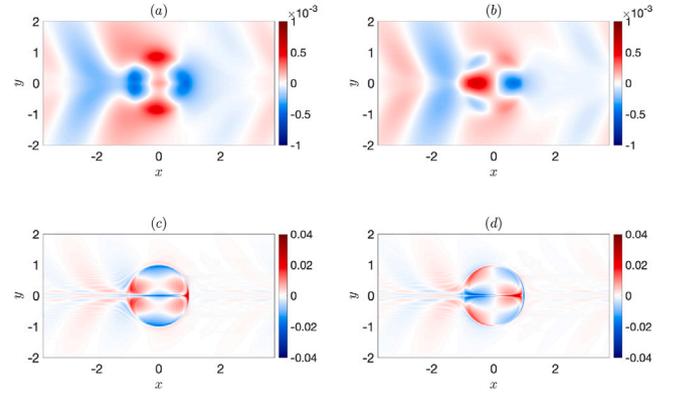
Fig. 2. Real (panels a and c) and imaginary (panels b and d) D-mode components, with the top row showing streamfunctions and the bottom row showing PVAs. Here, $\beta = 4c$, and our linear analysis associates this LRD with $(\sigma, \tau) = (0.027, 17)$.
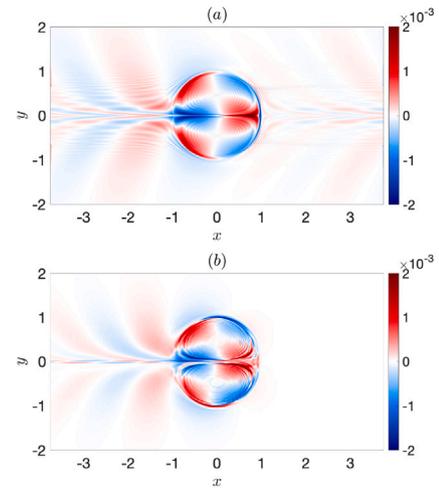
Fig. 3. Period-averaged PVA of the D-mode (multiplied by $e^{-\sigma t_1}$) with $\beta = 4c$: (a) is obtained using (18), with A and B as shown in Fig. 2, and with $(\sigma, \tau) = (0.027, 17)$; ($b$) is obtained from a series of QG model solution snapshots approximately over the D-mode period.

$t_1 + \tau$, when there was an intermediate stage of growth, finite snapshot comparison obtained from the high resolution numerical simulations deduced a value of $\tau_{\text{num}} \approx 16$ (the subscript num here refers to values associated with numerical simulations) and the growth between approximately periodic panels was calculated to be

$$\sigma_{\text{num}} = \frac{1}{\tau_{\text{num}}} \ln\left[\frac{\max(q_A(t_1 + \tau))}{\max(q_A(t_1))}\right] \approx 0.035. \tag{30}$$

The critical D-mode that develops on an LRD characterized by $\beta = 4c$ is described by our linear-stability analysis with $(\sigma, \tau) \approx (0.027, 17)$. Since this is similar to the previous breeding estimates, as well as to the D-mode spatial pattern (Fig. 3), this acts to support our results. Alternatively, differences in these values could be a consequence of differing resolutions assumed, and the value of σ might approach σ_{num} if the number of grid points were consistent between approaches.

An interesting characteristic feature of the D-mode is the trailing wake behind the LRD (Fig. 1). A similarly looking wake characterizes the viscous LCD, and it was hypothesized that it amplifies the dipole instability through the dipole-wake interaction [10]. On the contrary, we argue that the D-mode trailing wake is distinctly different, because of its inviscid nature. Further below, we argue that the presence of this wake is fundamentally important for the nonlinear mechanism that allows the D-mode to inevitably destroy the LRD.
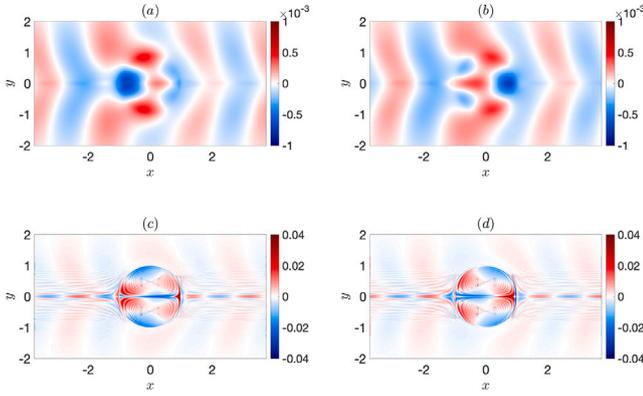
Fig. 4. Real (panels *a* and *c*) and imaginary (panels *b* and *d*) parts of the D-mode, with the top/bottom row showing streamfunction/PVA fields. Here, $\beta = 1.5c$ and $(\sigma, \tau) = (0.007, 20)$.

Additionally, with respect to increased dipole intensity, breeding results demonstrated decreasing linear growth rates (i.e., $\sigma_n \sim 0.027$ and $\sigma_n \sim 0.02$ for $\beta = 3c, 2c$, respectively), while the period of oscillation remained approximately uniform. In comparison, our linear instability solver extracted $(\sigma, \tau) \sim (0.015, 18)$ when $\beta = 3c$, and $(\sigma, \tau) \sim (0.009, 19)$ when $\beta = 2c$. This is consistent with decreasing linear growth, but also highlights a subtle increase in the oscillation period (see supplementary material for the streamfunction and PVA fields).

The numerical dipole studies [23,24] suggested a transition in dynamics for different values of β. In particular, when $\beta = (4, 3)c$ the LRD maintained steady propagation for awhile (longer in the more intense case) before succumbing to instability and destruction, whereas, when $\beta = 2c$, the LRD remained largely intact over the same time domain, but still noticeably decelerated. However, the $\beta = c$ dipole persists as an almost steadily drifting solution, thus, suggesting a bifurcation value, β_T, in the range $1 < \beta_T/c < 2$.

We considered a dipole intensity centred in this interval, $\beta/c = 1.5$, and obtained $(\sigma, \tau) \approx (0.007, 20)$ (see Fig. 4). Since this LRD still derives an unstable linear growth rate, this suggests that if a critical value for beta exists, it would be that $\beta_T/c < 1.5$. When $\beta = c$, we obtained $(\sigma, \tau) \approx (0.004, 21)$, however, the solution PVA field became noticeably noisy (see supplementary material), suggesting inadequate grid resolution. Nevertheless, this result is consistent with the hypothesis that progressively intensified LRDs are still linearly unstable, although instability growth rates continue to decay. To explore this further, the breeding may be the only affordable method, but it will require long-time integrations, and, therefore, even higher resolution to beat down numerical-viscosity effects.

4. Nonlinear analysis

4.1. Weakly nonlinear effects

To understand the key roles played by nonlinearity in the eastward dipole destruction, we considered eddy PV fluxes induced by the D-mode, as well as the energy transfer rate between the background dipole and the D-mode. This was done under the assumption that the nonlinear self-interaction of the D-mode is relatively weak, hence, the background dipole can be viewed as unchanged over one period of the growing D-mode. Mathematically, the zonal and meridional eddy PV flux components can be written as

$$F_x = -\partial_y \psi_A (q_A + \beta y),\tag{31}$$

$$F_y = \partial_x \psi_A (q_A + \beta y),\tag{32}$$

respectively, and related to the self-interaction of the D-mode described in terms of the eddy PV flux convergence (i.e., eddy forcing):

$$I = -\mathscr{J}(\psi_A, q_A + \beta y) = -\mathrm{div}(\boldsymbol{F}),\tag{33}$$

where $\boldsymbol{F} = (F_x, F_y)^T$. Note, that the above field contains small β-term, which would be averaged out over the oscillation period if ψ_A were not growing in time. Despite the fact that this field does grow over time, we found that the nonzero outcome of this is very small and insignificant, therefore, we omitted this contribution from further discussion. The field for I illustrates how the contents of dipole PV are redistributed by the action of the D-mode, while the flux components inform us of the corresponding PV pathways.

To understand the dipole destruction mechanism, we averaged the nonlinear self-interaction over a period of the D-mode oscillation and used this as a reference point for our discussion of the PV redistribution. In this case, it follows that

$$\overline{I} = \overline{\mathscr{J}(q_A, \psi_A)} - \beta \overline{\partial_x \psi_A},\tag{34}$$

where, using the normal-mode representation (16), we can write (see Appendix A.2 for a more detailed derivation):

$$\overline{\partial_x \psi_A} = \Lambda \partial_x \left[\sigma(Ac_1 - Bs_1) + \omega(As_1 - Bc_1) \right] e^{\sigma t_1},\tag{35}$$

and

$$\overline{\mathscr{J}(q_A, \psi_A)} = \frac{\Gamma}{\tau} \left[(\sigma^2 + \omega^2)(\mathscr{J}_{C,A} + \mathscr{J}_{D,B}) \right] \\ + \sigma \left[\delta_1(\mathscr{J}_{C,A} - \mathscr{J}_{D,B}) + \delta_2(\mathscr{J}_{A,D} + \mathscr{J}_{B,C}) \right],\tag{36}$$

with $\mathscr{J}_{a,b} = \mathscr{J}(a, b)$ and

$$C = \Delta A - \gamma^2 A, \\ D = \Delta B - \gamma^2 B.\tag{37}$$

Further, we introduced

$$\delta_1 = \sigma c_2(t_1) + \omega s_2(t_1), \\ \delta_2 = \sigma s_2(t_1) - \omega c_2(t_1),\tag{38}$$

and

$$\Gamma = \frac{e^{2\sigma\tau} - 1}{4\sigma(\sigma^2 + \omega^2)},\tag{39}$$

for the sake of compactness.

We found that the β-contribution was at least an order of magnitude smaller than the Jacobian term. Hence, we neglect it in the eddy forcing and flux components, hereafter. From Fig. 5, it is clear that each of these fields are odd with respect to the zonal axis. Moreover, Fig. 5*a* shows us how the PV content moves from left (negative blue regions) to right (positive red regions), while Fig. 5*b* conveys how PV is transferred up (positive red regions) and down (negative blue regions).

The eddy forcing (Fig. 5*c*) has a complicated structure that needs interpretation. Perhaps, a more informative way to appreciate it is through Fig. 6, where the integral values of $\overline{I}$ are presented for eight separate regions in the domain. From the distribution of values, it is clear that the upper (lower) region is negative (positive) dominant. In summary, this can be interpreted as the D-mode reducing the PV contrast in the dipole (we refer to this as *PV decontrasting*, which we use to mean that PV from one partner invades the other). To investigate this, we added a small perturbation of this structure to the LRD and showed that its intensity directly influences and shortens the dipole lifetime. Such a result is consistent with our PV decontrasting hypothesis.

The arrows in Fig. 6 correspond to the net eddy PV flux along each of the zonal and meridional central lines; the size of the arrows is not to scale, but does represent the magnitude of flux in a particular direction. Hence, the main transfer route contributing to PV decontrasting through meridional PV rearrangement occurs near the trailing saddle
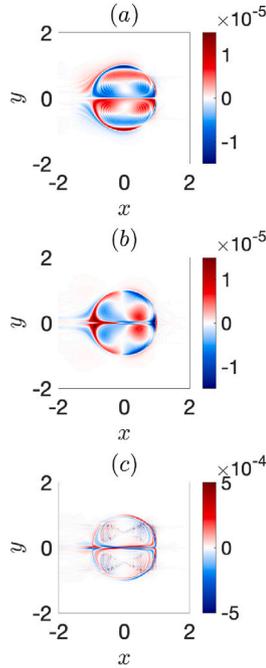
Fig. 5. Nonlinear properties of the D-mode: (a) zonal eddy PV flux $\overline{F_x}$, (b) meridional eddy PV flux $\overline{F_y}$, (c) eddy forcing I.
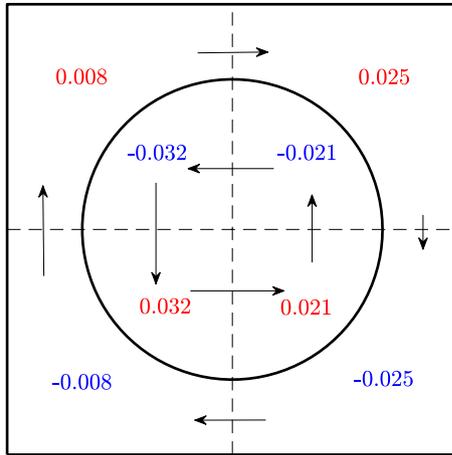
Fig. 6. Integral-value diagram corresponding to $\overline{I}$, describing how the overall PV content is rearranged due to a growing D-mode, and as a result of its nonlinear self-interaction (i.e., eddy forcing). The size of arrows is not to scale, but describes the net eddy PV flux in the horizontal and meridional directions across the zonal and meridional segments. The circular boundary has unit radius corresponding to the initial separatrix of the dipole.

point at $x = -1$ along the zonal axis and is described by negative eddy PV flux. Part of the corresponding PV gets recycled by returning back through the net cyclonic (counter-clockwise) circulation of PV inside the dipole, informing us that the D-mode also zonally rearranges PV. This dynamical behaviour can explain the zonal elongations observed in [23,24], since this rearrangement of PV content in the dipole can cause deformations along the dipole axis.

The 8 values corresponding to the 8 subdomains in Fig. 6 correspond to the net area-integrated eddy PV flux convergences induced by the D-mode. This is a compact description of the D-mode rearrangement of the dipole PV content. Fig. 6 summarizes a PV decontrasting effect, that is, the PV contrast in the dipole becomes reduced; thus, irreversible PV

stirring induced by the D-mode acts to destroy the dipole. Now that we understand how the D-mode alters the dipole, we proceed to explain the corresponding amplification process by using energy arguments in the following subsection.

4.2. D-mode energetics

We derived equations for the energy balance by considering the background LRD and the perturbation D-mode evolving on it. For this purpose, we use the method of multiple scales to separate the fast time scale of D-mode oscillation, T_f, from the slow time scale associated with deviations in the LRD, T_s. Hence, this suggests the following Reynolds decomposition of the streamfunction:

$$\psi = \overline{\psi}(x, y, T_s) + \psi_A(x, y, T_s, T_f), \tag{40}$$

where the first term is approximately the LRD field. Substituting into the perturbation governance (22), we obtained

$$\partial_{T_s}\overline{q} + \partial_{T_s}q_A + \partial_{T_f}q_A + \mathscr{J}(\overline{\psi}, \Delta\overline{\psi}) + \mathscr{J}(\overline{\psi}, \Delta\psi_A) \\ + \mathscr{J}(\psi_A, \Delta\overline{\psi}) + \mathscr{J}(\psi_A, \Delta\psi_A) + \beta\partial_x(\overline{\psi} + \psi_A) = 0, \tag{41}$$

which can be multiplied by $\overline{\psi}$ and integrated over $t_1 \le t \le t_1 + \tau$, to derive:

$$\overline{\psi}\partial_{T_s}\overline{q} + \overline{\psi}\,\mathscr{J}(\overline{\psi}, \Delta\overline{\psi}) + \overline{\psi}\,\overline{\mathscr{J}(\psi_A, \Delta\psi_A)} + \beta\overline{\psi}\partial_x\overline{\psi} = 0. \tag{42}$$

Here, we note that $\overline{\psi_A}, \overline{q_A}$ are very small relative to $\overline{\psi}$, meaning that linear combinations with respect to average A-components can be neglected when considering terms of order $\overline{\psi}$ (however, the scale of nonlinear combinations is unclear and cannot be neglected). Thus, further manipulation yields the energy balance,

$$\partial_{T_s}E_S = \mathrm{div}(\mathbf{Q}_S) + \mathscr{L}, \tag{43}$$

where $\mathbf{Q}_S$ is the mean energy flux, and

$$\mathscr{L} = \partial_{xy}\overline{\psi}\left[\overline{(\partial_x\psi_A)^2} - \overline{(\partial_y\psi_A)^2}\right] + \overline{\partial_x\psi_A\partial_y\psi_A}(\partial_{yy}\overline{\psi} - \partial_{xx}\overline{\psi}), \tag{44}$$

is the LRD/D-mode energy exchange (or transfer) term. Similarly, we multiplied (41) by ψ_A and averaged over the period of oscillation to obtain the perturbation energy equation,

$$\partial_{T_s}E_A = \mathrm{div}(\mathbf{Q}_A) - \mathscr{L}, \tag{45}$$

where $\mathbf{Q}_A$ is the perturbation energy flux. Since the exchange term $\mathscr{L}$ appears in both (43) and (45) with opposite sign value, this describes an exchange of energy between the background flow and the perturbation field.

We can recast the energy exchange using the normal mode representation for ψ_A to obtain

$$\mathscr{L} = \frac{\Gamma}{4\tau}\left\{ 4(\sigma^2 + \omega^2)(\Phi_1 F_1 + \Phi_2 F_3) \\ + \sigma\left[\delta_1(\Phi_1 F_2 + \Phi_2 F_4) + \delta_2(\Phi_2 F_6 - 2\Phi_1 F_5)\right]\right\} e^{2\sigma t_1}, \tag{46}$$

where

$$\begin{aligned} F_1 &= (\partial_x A)^2 - (\partial_y A)^2 + (\partial_x B)^2 - (\partial_y B)^2, \\ F_2 &= (\partial_x A)^2 - (\partial_y A)^2 - (\partial_x B)^2 + (\partial_y B)^2, \\ F_3 &= \partial_x A\partial_y A + \partial_x B\partial_y B, \\ F_4 &= \partial_x A\partial_y A - \partial_x B\partial_y B, \\ F_5 &= \partial_x A\partial_x B - \partial_y A\partial_y B, \\ F_6 &= \partial_x A\partial_y B + \partial_y A\partial_x B, \end{aligned} \tag{47}$$

and

$$\begin{aligned} \Phi_1 &= \partial_{xy}\overline{\psi}, \\ \Phi_2 &= \partial_{yy}\Psi - \partial_{xx}\overline{\psi}. \end{aligned} \tag{48}$$
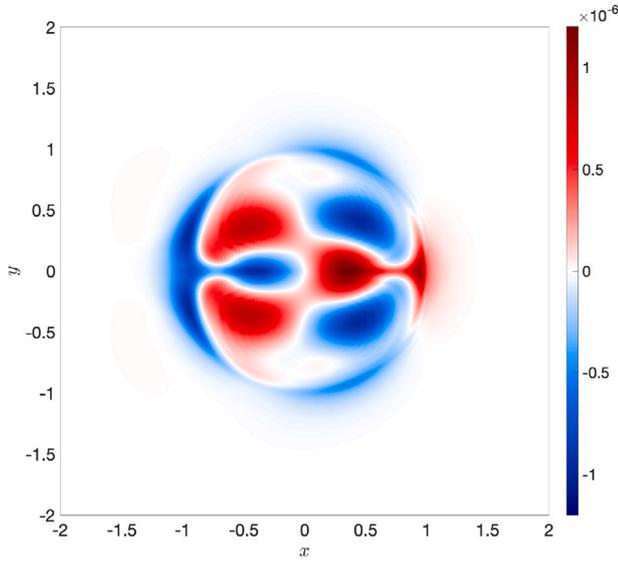
Fig. 7. Energy transfer between the background dipole and the D-mode, averaged over a time period of the latter. Negative regions correspond to energy extracted from the dipole by the D-mode, while positive regions correspond to energy transferred back to the dipole. Domain-integrated energy transfer is negative, which is consistent with the growing instability.
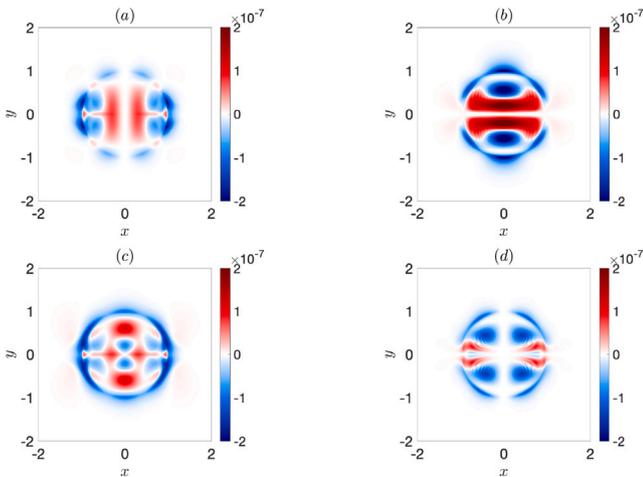
Fig. 8. Components of the energy exchange in Fig. 7, in terms of M- and N-components: (a) $(MN)_x$; (b) $(MN)_y$; (c) $(NM)_x$; (d) $(NM)_y$.

Using (46), we plot the energy exchange contribution in Fig. 7. This clearly shows an antisymmetric pattern with respect to the meridional axis, where positive regions correspond to background flow energy being returned to the dipole, whereas, negative regions refer to energy extraction from the background flow by the perturbation field. The latter of these prevails and can be interpreted as energy extracted by the D-mode as part of the nonlinear destruction of the dipole. An important note is that the D-mode extracts energy near the rear saddle point (while the dipole gains energy at the frontal lobe), which is consistent with the majority of flux exchange contributing to the PV decontrasting of the dipole by eddy PV flux being local to this saddle point.

4.3. Asymmetry analysis of nonlinear effects

By construction, the critical D-mode has even symmetry about the zonal axis, however, no assumption is made about the symmetry across the meridional axis. Since there is meridional asymmetry in the average nonlinear self-interaction and the energy exchange fields, we are

motivated to check whether it is essential for the nonlinear destruction of the dipole. We analyse this by introducing M- and N-components, such that:

$$\psi_M = \frac{\psi_A(x, y, t) + \psi_A(-x, y, t)}{2}, \tag{49}$$

$$\psi_N = \frac{\psi_A(x, y, t) - \psi_A(-x, y, t)}{2}, \tag{50}$$

where the M- and N-component are field with even and odd symmetry, respectively, about the meridional axis. We define $q_{M,N}$ in a similar way, then the term describing energy exchange is expanded as

$$
\begin{aligned}
\mathcal{L} = & \overline{\partial_x \psi_M \, \mathscr{J}(\psi_M, \partial_x \overline{\psi})} + \overline{\partial_x \psi_M \, \mathscr{J}(\psi_N, \partial_x \overline{\psi})} \\
& + \overline{\partial_x \psi_N \, \mathscr{J}(\psi_M, \partial_x \overline{\psi})} + \overline{\partial_x \psi_N \, \mathscr{J}(\psi_N, \partial_x \overline{\psi})} \\
& + \overline{\partial_y \psi_M \, \mathscr{J}(\psi_M, \partial_y \overline{\psi})} + \overline{\partial_y \psi_M \, \mathscr{J}(\psi_N, \partial_y \overline{\psi})} \\
& + \overline{\partial_y \psi_N \, \mathscr{J}(\psi_M, \partial_y \overline{\psi})} + \overline{\partial_y \psi_N \, \mathscr{J}(\psi_N, \partial_y \overline{\psi})}.
\end{aligned}
\tag{51}
$$

Each of the eight contributions in (51) is either symmetric in both horizontal directions, or contains antisymmetry in one of the directions. A consequence of antisymmetry is that the net spatial integral is zero, which eliminates half of the contributions in (51).

In summary, the surviving integral contributors are given by (see Fig. 8):

$$
\begin{aligned}
(MN)_x &= \overline{\partial_x \psi_M \, \mathscr{J}(\psi_N, \partial_x \overline{\psi})}, \\
(MN)_y &= \overline{\partial_y \psi_M \, \mathscr{J}(\psi_N, \partial_y \overline{\psi})}, \\
(NM)_x &= \overline{\partial_x \psi_N \, \mathscr{J}(\psi_M, \partial_x \overline{\psi})}, \\
(NM)_y &= \overline{\partial_y \psi_N \, \mathscr{J}(\psi_M, \partial_y \overline{\psi})}.
\end{aligned}
\tag{52}
$$

Each of these fields have negative net integrals over the spatial domain, which corresponds to the D-mode gaining energy and becoming destabilized. Hence, the nonlinear destruction mechanism fundamentally involves west–east asymmetry of the D-mode, that is most vividly expressed by the trailing wake behind the dipole.

We can interpret this wake as a set of coherently radiating Rossby waves, which are themselves a consequence of the broken west–east symmetry by the β-effect. Without this asymmetry the D-mode is not capable of the down-gradient PV stirring that "cools down" the dipole and extracts its energy for this work.

5. Summary and discussion

This work is demonstration of methodology for future studies of stability and dynamics of isolated coherent vortices without simplifying spatial symmetries, such as ubiquitous vortices in geophysical fluids (i.e., in oceans and atmospheres). These vortices transport and redistribute important fluid properties, such as heat, momentum and material tracers, and, therefore, largely shape up general circulations. Taxonomy, generation, dynamics, life cycles and impacts of the vortices remain only partially understood despite many decades of research.

We pose the problem in terms of oceanic mesoscale vortices and consider shallow-water upper-ocean intensified vortices at midlatitudes of a rotating planet and far away from continental boundaries. All together, this amounts to considering classical QG, equivalent-barotropic dynamics in a 2D double-periodic domain, which is taken to be a lot larger than the isolated coherent vortex dipole being considered. The main motivations are to extract the growing instability in terms of the critical normal mode and to understand the mechanisms by which this mode destroys the dipole.

With the above motivations and formulation in mind, we focused on the linear instability and weakly nonlinear dynamics of coherent, eastward-propagating, steady-state Larichev–Reznik vortex dipole (LRD), which is a classical asymptotic QG solution of rotating shallow-water model, and explored it in terms of linear critical normal-mode analysis. Absence of azimuthal symmetry in the LRD makes such analysis problematic, even computationally, therefore, it has remained undone until now.

To extract the critical mode, we applied both breeding methodology based on solving initial-value problem and brute-force, direct full-spectrum eigenproblem formulation involving large-size matrices. The latter approach made use of the second-order central finite-difference discretization, allowed us to solve for the entire eigenspectrum, and yielded results consistent with those obtained in [23]. The dipoles were found to be linearly unstable, with characteristic decrease (increase) in growth rate (oscillation period) with respect to increase in dipole intensity.

Next, we considered nonlinear self-interaction and energetics of the growing critical D-mode and its induced eddy PV fluxes and their convergence, that is, eddy forcing, as well as we also considered the mechanical energy balance involving energy transfer between the dipole and D-mode. These analyses revealed that the critical mode destroys the dipole by extracting its energy and stirring its PV content in the down-gradient sense, thus, reducing the PV contrast in the dipole and providing physical mechanisms of the dipole destruction. Details of this process were uncovered and the fundamental importance of the west-east zonal asymmetry of the D-mode was demonstrated.

The key aspect of our approach is the use of linear, critical normal modes to solve accurately for all relevant physical fields that illuminate the involved mechanisms. Based on the insight we gained by employing our linear and nonlinear analyses, we anticipate the use of similar linear instability solvers and normal mode representations to extract critical modes for other kinds of dipoles and coherent vortices. This includes those in the presence of topographic features, those obtained in a full rather than asymptotic shallow-water model, those exposed to background flow effects and more realistic stratification.

A drawback of our linear-stability analysis is the limited spatial resolution we are constrained by to solve the discretized eigenproblem. This is a consequence of our method solving for the entire eigenspectrum, rather than only solving for the critical mode and its neighbours in terms of the growth rates. In the future, we envision the application of eigenproblem methods that only extract a few leading eigenmodes (e.g., Arnoldi iterations in Krylov subspaces). The benefit of such approaches is that finer resolution can be employed, leading to greater accuracy when discussing the top modes.

On the other hand, as shown, the breeding method can work with decent accuracy for the critical mode only. Finally, our analysis showed that the rear (and to the lesser degree frontal) saddle point along the separatrix of the LRD seems to be the gateway for important meridional PV eddy flux. Despite this, we did not expand on why these points play these particular roles and left the issue for future studies. The methodology for gaining further insight into this is tracking Lagrangian particles and contours, as in the theory of lobe dynamics [32], which works well for analysis of material transport around saddle points in time-dependent flows.

Declaration of competing interest

The authors declare the following financial interests/personal relationships which may be considered as potential competing interests: Jack Davies reports financial support was provided by Imperial College London. If there are other authors, they declare that they have no known competing financial interests or personal relationships that could have appeared to influence the work reported in this paper.

Data availability

Data will be made available on request.

Appendix A

A.1. Matrix formulation

Here, we present some technical details pertaining to the derivation of the eigenproblem (26). We make use of the second-order central finite-difference discretizations of the derivatives:

$$\partial_x \Psi_{i,j} \approx \frac{\Psi_{i+1,j} - \Psi_{i-1,j}}{2h},$$

$$\partial_y \Psi_{i,j} \approx \frac{\Psi_{i,j+1} - \Psi_{i,j-1}}{2h},$$

$$\Delta \Psi_{i,j} \approx \frac{\Psi_{i+1,j} + \Psi_{i-1,j} + \Psi_{i,j+1} + \Psi_{i,j-1} - 4\Psi_{i,j}}{h^2},$$

$$\partial_x \Delta \Psi_{i,j} \approx \frac{1}{h^3}\left[2(\Psi_{i-1,j} - \Psi_{i+1,j}) + \frac{1}{2}(\Psi_{i+2,j} - \Psi_{i-2,j})\right.$$
$$\left. + \Psi_{i+1,j-1} - \Psi_{i-1,j-1} + \Psi_{i+1,j+1} - \Psi_{i-1,j+1})\right],$$

$$\partial_y \Delta \Psi_{i,j} \approx \frac{1}{h^3}\left[2(\Psi_{i,j-1} - \Psi_{i,j+1}) + \frac{1}{2}(\Psi_{i,j+2} - \Psi_{i,j-2})\right.$$
$$\left. + \Psi_{i+1,j+1} - \Psi_{i+1,j-1} + \Psi_{i-1,j+1} - \Psi_{i-1,j-1})\right],$$

where $h = L_x/N$. Substituting these stencils into (25), the non-zero elements of $\mathbf{M}$ are:

$$\Psi_{i+1,j+1} : \quad \frac{-\partial_x \psi + \partial_y \psi + c}{2h^3},$$

$$\Psi_{i+1,j-1} : \quad \frac{\partial_x \psi + \partial_y \psi + c}{2h^3},$$

$$\Psi_{i-1,j+1} : \quad \frac{-\partial_x \psi - \partial_y \psi - c}{2h^3},$$

$$\Psi_{i-1,j-1} : \quad \frac{\partial_x \psi - \partial_y \psi - c}{2h^3},$$

$$\Psi_{i+2,j} : \quad \frac{\partial_y \psi + c}{2h^3},$$

$$\Psi_{i-2,j} : \quad \frac{-\partial_y \psi - c}{2h^3},$$

$$\Psi_{i,j+2} : \quad -\frac{\partial_x \psi}{2h^3},$$

$$\Psi_{i,j-2} : \quad \frac{\partial_x \psi}{2h^3},$$

$$\Psi_{i+1,j} : \quad -\frac{\sigma}{h^2} - \frac{\gamma^2(\partial_y \psi + c)}{2h} - \frac{(\partial_y q + \beta)}{2h} - \frac{2(\partial_y \psi + c)}{h^3},$$

$$\Psi_{i-1,j} : \quad -\frac{\sigma}{h^2} + \frac{\gamma^2(\partial_y \psi + c)}{2h} + \frac{(\partial_y q + \beta)}{2h} + \frac{2(\partial_y \psi + c)}{h^3},$$

$$\Psi_{i,j+1} : \quad -\frac{\sigma}{h^2} + \frac{2\partial_x \psi}{h^3} + \frac{\gamma^2 \partial_x \psi}{2h} + \frac{\partial_x q}{2h},$$

$$\Psi_{i,j+1} : \quad -\frac{\sigma}{h^2} - \frac{2\partial_x \psi}{h^3} - \frac{\gamma^2 \partial_x \psi}{2h} - \frac{\partial_x q}{2h},$$

and the non-zero elements of $\mathbf{N}$ are:

$$\Psi_{m,j} : \quad \frac{\omega}{h^2}, \quad \text{for} \quad m = i \pm 1,$$

$$\Psi_{i,n} : \quad \frac{\omega}{h^2}, \quad \text{for} \quad n = j \pm 1.$$

This system is solved using doubly-periodic boundary conditions. In practice, since we hunted for the critical D-mode, which is asymmetric around the zonal axis, the eigenproblem has been solved in the lower half of the domain with the asymmetry built into the boundary condition at the zonal axis.

A.2. Normal mode equations

Here, we derive equations for the nonlinear interaction of the D-mode. First, we note that terms due to β are relatively small, so we consider:

$$\mathcal{J}(\psi_A, q_A) = \partial_x F_x + \partial_y F y.$$

The flux components are rewritten as

$$F_x = \left[-\partial_y A C c_1^2 + (\partial_y A D + \partial_y B C) c_1 s_1 - \partial_y B D s_1^2 \right] e^{2\sigma t},$$

$$F_y = \left[\partial_x A C c_1^2 - (\partial_x A D + \partial_x B C) c_1 s_1 + \partial_x B D s_1^2 \right] e^{2\sigma t},$$

which means that

$$\partial_x F_x = \left[-(\partial_{xy} A C + \partial_y A \partial_x C) c_1^2 + (\partial_{xy} A D + \partial_y A \partial_x D \right.$$
$$\left. + \partial_{xy} B C \partial_y B \partial_x C) c_1 s_1 - (\partial_{xy} B D + \partial_y B \partial_x D) s_1^2 \right] e^{2\sigma t},$$

$$\partial_y F_y = \left[(\partial_{xy} A C + \partial_x A \partial_y C) c_1^2 - (\partial_{xy} A D + \partial_x A \partial_y D \right.$$
$$\left. + \partial_{xy} B C \partial_x B \partial_y C) c_1 s_1 + (\partial_{xy} B D + \partial_x B \partial_y D) s_1^2 \right] e^{2\sigma t},$$

$$\mathcal{J}(\psi_A, q_A) = \left[\mathcal{J}_{A,C} c_1^2 + (\mathcal{J}_{D,A} + \mathcal{J}_{C,B}) c_1 s_1 + \mathcal{J}_{B,D} s_1^2 \right] e^{2\sigma t}.$$

To integrate over a period of oscillation, we make use of the following integrals,

$$\int_{t_1}^{t_1+\tau} c_1^2 e^{2\sigma t} \, dt = \Gamma(\sigma^2 + \omega^2 + \sigma\delta_1) e^{2\sigma t_1},$$

$$\int_{t_1}^{t_1+\tau} s_1^2 e^{2\sigma t} \, dt = \Gamma(\sigma^2 + \omega^2 - \sigma\delta_1) e^{2\sigma t_1},$$

$$\int_{t_1}^{t_1+\tau} c_1 s_1 e^{2\sigma t} \, dt = \sigma\delta_2 \Gamma e^{2\sigma t_1},$$

and derive the equations:

$$\overline{\partial_x F_x} = \frac{\Gamma}{\tau} \left\{ -(\sigma^2 + \omega^2)(\partial_{xy} A C + \partial_y A \partial_x C + \partial_{xy} B D + \partial_y B \partial_x D) \right.$$
$$+ \sigma \left[\delta_1(\partial_{xy} B D + \partial_y B \partial_x D - \partial_{xy} A C - \partial_y A \partial_x C) \right.$$
$$\left. \left. + \delta_2(\partial_{xy} A D + \partial_y A \partial_x D + \partial_{xy} B C \partial_y B \partial_x C) \right] \right\} e^{2\sigma t_1},$$

$$\overline{\partial_y F_y} = \frac{\Gamma}{\tau} \left\{ (\sigma^2 + \omega^2)(\partial_{xy} A C + \partial_x A \partial_y C + \partial_{xy} B D + \partial_x B \partial_y D) \right.$$
$$+ \sigma \left[\delta_1(\partial_{xy} A C + \partial_x A \partial_y C - \partial_{xy} B D - \partial_x B \partial_y D) \right.$$
$$\left. \left. - \delta_2(\partial_{xy} A D + \partial_x A \partial_y D + \partial_{xy} B C \partial_x B \partial_y C) \right] \right\} e^{2\sigma t_1},$$

and

$$\overline{\mathcal{J}(\psi_A, q_A)} = \frac{\Gamma}{\tau} \left\{ (\sigma^2 + \omega^2)(\mathcal{J}_{A,C} + \mathcal{J}_{B,D}) \right.$$
$$\left. + \sigma \left[\delta_1(\mathcal{J}_{A,C} - \mathcal{J}_{B,D}) + \delta_2(\mathcal{J}_{D,A} + \mathcal{J}_{C,B}) \right] \right\}.$$

Note that the derivation of the energy transfer between the background dipole and D-mode perturbations is similar.

Appendix B. Supplementary data

Supplementary material related to this article can be found online at https://doi.org/10.1016/j.physd.2024.134068.

References

[1] V. Kamenkovich, M. Koshlyakov, A. Monin, Synoptic Eddies in the Ocean. EFM, D, vol. 62, Reidel Publ. Company, Dordrecht, 1986, p. 433.
[2] J.C. McWilliams, J.B. Weiss, Chaos 4 (2) (1994) 305–311.
[3] J.C. McWilliams, J. Fluid Mech. 146 (1984) 21–43.
[4] A.P. Ingersoll, Science 248 (4953) (1990) 308–315.
[5] L. Bengtsson, J. Lighthill, Intense Atmospheric Vortices: Proceedings of the Joint Symposium, IUTAM/IUGG Held At Reading (United Kingdom) July 14–17, 1981, Springer Science & Business Media, 2013.
[6] T. Dowling, E. Spiegel, Ann. New York Acad. Sci. (USA) 617 (CONF-8910308-) (1990).
[7] H. Lamb, Hydrodynamics, second ed., Cambridge University Press, 1895.
[8] V. Meleshko, G. Van Heijst, J. Fluid Mech. 272 (1994) 157–182.
[9] R. Khvoles, D. Berson, Z. Kizner, J. Fluid Mech. 530 (2005) 1–30.
[10] V. Brion, D. Sipp, L. Jacquin, Phys. Fluids 26 (6) (2014) 064103.
[11] M. E. Stern, J. Mar. Res. 33 (1975) 1–13.
[12] Z. Kizner, D. Berson, J. Mar. Res. 58 (3) (2000) 375–403.
[13] V. Larichev, G.M. Reznik, Doklady Akademii Nauk, vol. 231, (no. 5) Russian Academy of Sciences, 1976, pp. 1077–1079.
[14] G. Reznik, Izv. Atmos. Ocean. Phys. 46 (6) (2010) 784–797.
[15] J.C. McWilliams, Dyn. Atmos. Oceans 5 (1) (1980) 43–66.
[16] N. Butchart, K. Haines, J. Marshall, J. Atmos. Sci. 46 (13) (1989) 2063–2078.
[17] J. Nycander, Phys. Fluids A Fluid Dyn. 4 (3) (1992) 467–476.
[18] G.E. Swaters, G.R. Flierl, Elsevier Oceanography Series, vol. 50, Elsevier, 1989, pp. 149–165.
[19] J.C. McWilliams, G.R. Flierl, V.D. Larichev, G.M. Reznik, Dyn. Atmos. Oceans 5 (4) (1981) 219–238.
[20] G.F. Carnevale, G.K. Vallis, R. Purini, M. Briscolini, Geophys. Astrophys. Fluid Dyn. 41 (1–2) (1988) 45–101.
[21] S. Muzylev, G. Reznik, Phys. Fluids B Plasma Phys. 4 (9) (1992) 2841–2844.
[22] G.E. Swaters, Stud. Appl. Math. 112 (3) (2004) 235–258.
[23] J. Davies, G.G. Sutyrin, P. Berloff, Phys. Fluids 35 (4) (2023).
[24] J. Davies, G.G. Sutyrin, M. Crowe, P. Berloff, Phys. Fluids 35 (11) (2023).
[25] P. Berloff, S. Meacham, J. Mar. Res. 56 (5) (1998) 937–993.
[26] I. Shevchenko, P. Berloff, D. Guerrero-López, J. Roman, J. Fluid Mech. 795 (2016) 423–442.
[27] J. Pedlosky, et al., Geophysical Fluid Dynamics, vol. 710, Springer, 1987.
[28] G.K. Vallis, Atmospheric and Oceanic Fluid Dynamics, Cambridge University Press, 2017.
[29] E. Johnson, M. Crowe, J. Fluid Mech. 958 (2023) R2.
[30] Z. Toth, E. Kalnay, Bull. Am. Meteorol. Soc. 74 (12) (1993) 2317–2330.
[31] B. Farrell, J. Atmos. Sci. 41 (4) (1984) 668–673.
[32] N. Malhotra, S. Wiggins, J. Nonlinear Sci. 8 (1998) 401–456.